

A simple optical system for real-time size measurements of TRISO fuel pellets

Thomas P. Karnowski, Andrew K. Kercher, John D. Hunn, L. Curt Maxey
Oak Ridge National Laboratory, Bethel Valley Road, Oak Ridge TN 37831

ABSTRACT

Oak Ridge National Laboratory (ORNL) has begun the development of a program for the manufacturing and characterizing fuel pellets for use in advanced nuclear reactors. To achieve high reliability it is necessary to characterize the pellets during production runs. In this paper we present a simple TRISO Particle Counting And Sizing Tool (TP-CAST) that performs dual measurements of counting and size estimation for particles at rates up to 200 per second. The TP-CAST is based on a laser with line-generation optics and a PC-based data acquisition and analysis system. The instrument can measure 1000 micron pellets with a standard deviation of approximately 11 microns and with counting errors less than 0.075%. Our paper discusses the signal modeling, algorithms for size estimation, system design, and experimental results of the prototype TP-CAST system assembled at ORNL.

INTRODUCTION

Advanced nuclear reactor designs use fuel forms that are built up from tens of thousands of coated TRISO particles. These particles employ a dense layer of silicon carbide to trap radioactive fission products. These advanced reactors operate at gas temperatures around 900°C and can produce 30% more energy than today's pressurized-water reactors. The coated TRISO fuel acts as a containment system to prevent the release of fission products to the environment during accidents [1]. A diagram of one type of TRISO particle is shown in Figure 1 [2].

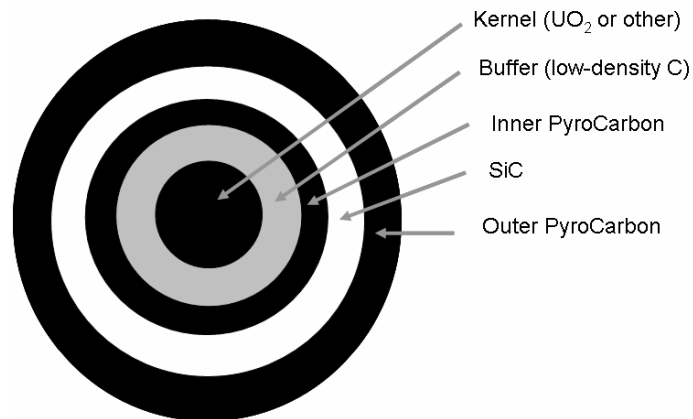


Figure 1. Diagram of example TRISO fuel pellet.

Rapid counting and measurement of TRISO spheres is a necessary technology for the development of these materials. A survey of commercial equipment found available devices lacking in both resolution and accuracy. We therefore elected to develop this capability in-house. Our instrument, the TRISO Particle Counting And Sizing Tool (TP-CAST) measures particles between 300 microns and 1000 microns in diameter. High counting accuracy and speed is desired, with a goal of counting a large batch of 1,000,000 in approximately 2 hours with errors on the order of 1 per 1000 particles counted.

Based on the methods used by Wallisch and Koss [3] we employed a light obstruction concept where a slit of light (either an aperture or a focused beam) is blocked by a particle. We assume the slit is small so only a single particle is in the slit at any given time. Other more recent work in quantifying TRISO particles has featured digital microphotography [4] and combinations of ultrasonic, optical and magnetic measurements [5].

The TP-CAST consists of an optical system that projects light through a target transport cell and collects the light onto a photo receiver (Figure 2). The signal from the photo receiver is digitized by a high-speed ADC unit and is processed in real-time. The events are counted and each event is analyzed to estimate the size of the particle. The particles are pulled via a vacuum through a small piece of tygon tubing, shot through the target cell which is fitted with an optical window, and collected with a cyclonic separator.

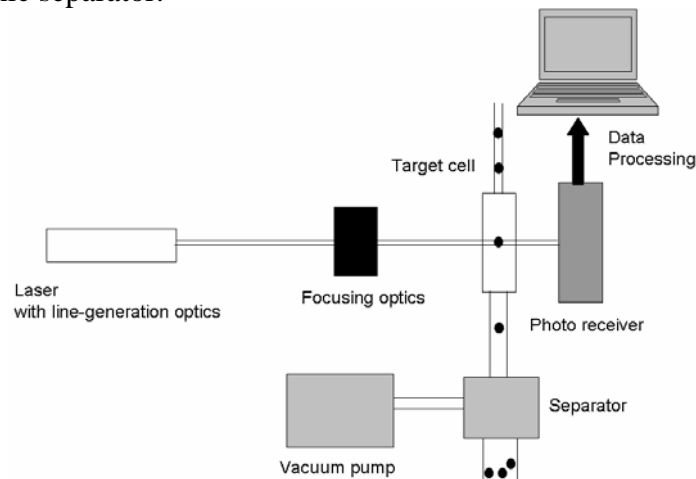


Figure 2. Diagram of TP-CAST

In this paper we present analytical techniques to estimate the size of the particles from the obstruction signal. We estimate the error from each technique and explore some of the sources of error in the optical implementation. We then show the elements of the system design. Finally, we present experimental results obtained with the particle size analyzer.

SIGNAL MODELING

A sphere moving past a slit of light produces a signal which starts high, shrinks as the sphere enters the light, reaches a minimum as the sphere blocks the maximum light, and then grows as the sphere

leaves the slit. We first focus on determining an expression for the area blocked by a circle passing by a slit. We assume that the sphere, radius R , is moving in the x -direction with constant velocity (v). Let the slit have thickness (h) which is less than the diameter of the sphere (see Figure 3). Since the circular shadow of the sphere is symmetric around the x axis, we express the intersection of the slit at position vt with the circle as the definite integral of the circle over the width of the slit,

$$\int_{vt - \frac{h}{2}}^{vt + \frac{h}{2}} 2\sqrt{R^2 - x^2} dx . \quad \text{Equation 1}$$

(We are ignoring the regions where $|vt| - h/2 > R$.) The solution to the integral is:

$$R^2 \left(\sin^{-1} \left(\frac{vt + \frac{h}{2}}{R} \right) - \sin^{-1} \left(\frac{vt - \frac{h}{2}}{R} \right) \right) + \left(vt + \frac{h}{2} \right) \sqrt{R^2 - \left(vt + \frac{h}{2} \right)^2} - \left(vt - \frac{h}{2} \right) \sqrt{R^2 - \left(vt - \frac{h}{2} \right)^2} \quad \text{Equation 2}$$

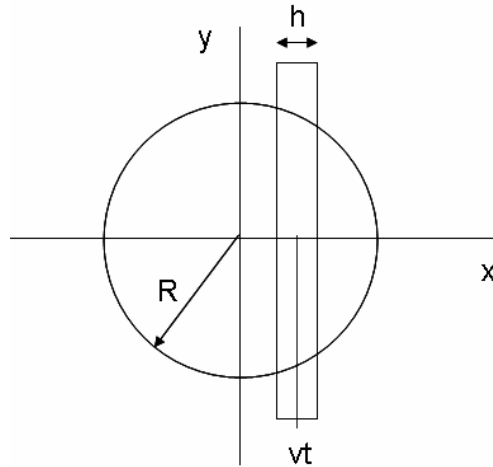


Figure 3. Slit of size h blocking a circle of radius R .

The function will be at a maximum when $t=0$, and will have a value of

$$R^2 \left(2 \sin^{-1} \left(\frac{h}{2R} \right) \right) + h \sqrt{R^2 - \frac{h^2}{4}} . \quad \text{Equation 3}$$

If h is small relative to R , we find that we can approximate $\sin^{-1}\left(\frac{h}{2R}\right) \approx \frac{h}{2R}$, and

$h\sqrt{R^2 - \frac{h^2}{4}} \approx h\sqrt{R^2}$ to give a maximum value at $t=0$ of $2hR$. Thus we see the peak is proportional to the diameter. To find the impact of the approximation, we determine our signal in the limit as h becomes an infinitely small slit. Let the area obstructed by the circle be approximated by the length of a line drawn through the circle, perpendicular to the direction of sphere travel. Assuming the light intensity is B , the length of the slit is L , velocity v , and time t , the light level is

$$B\left(L - 2\sqrt{R^2 - v^2t^2}\right), \text{ for } |vt| \leq R ; BL \text{ elsewhere.} \quad \text{Equation 4}$$

We suggest three ways to estimate the particle size after subtracting the baseline level $B \times L$:

1. From the extrema of the signal which is proportional to R . We call this the “peak” method.
2. After subtracting from $B \times L$, squaring the remaining values removes the radical term and allows us to solve a linear system for v^2 and R^2 . We call this the “square” method.
3. Finally, the integral of Equation 4 is proportional to the area of the circular shadow of the particle. Thus we can solve for R by summing up samples of the signal. Since the integral will also be proportional to the velocity v , we must use an estimate of v in this method. We call this the “integral” method.

SYSTEM DESIGN

Based on our specifications, we elected not to pursue a digital camera solution. An early concept utilized a 4096 pixel line-scan camera operating at 20 kHz, but this was deemed too expensive and lacking sufficient sensitivity, as we estimated it would only allow approximately 100 measurement lines per particle. We therefore elected to pursue a system more like that of [3].

We used a Stocker-Yale Microfocus laser, part number MFL-650S-10-15-185-SD as the optical source. This unit operates at a visible wavelength of 650 nm and has a 15 degree fan angle, with an ideal focal distance of 185 mm. At this focus point, the laser beam has a thickness of approximately 35 microns.

We used a New Focus Model 2032 wide-area, free-space visible light photo receiver. To match the quantized gains of our ADC unit we used the middle gain setting and also incorporated a neutral density filter with an optical density of 0.6. This filter fits into a holder on the 2032.

We used a National Instruments 6111E general-purpose data acquisition card for our ADC unit with a sampling rate of 5 MHz. The unit offers DAC outputs, which proved useful for testing and debugging the data acquisition software. The ADC is a 12 bit unit but is bipolar only. Because our signal is positive-valued, we only have 11 bits available.

We use a 100 mm cylindrical lens to collimate the expanding beam from the laser. This keeps the beam at a constant width and also helps prevent the fan angle problem discussed later.

The particle handling system consists of tygon tubing, a target cell, a vacuum pump, and a cyclonic separator. The cell has a small inlet tube on the top and a larger outlet tube on the bottom. Particles are drawn through the tygon tubing by the vacuum pump where they enter into the cell and pass through a chamber 1500 microns wide and deep. Two windows on the chamber permit the laser line to pass through the cell to detect the particle.

The experimental and final instruments are shown in Figure 4 and Figure 5.

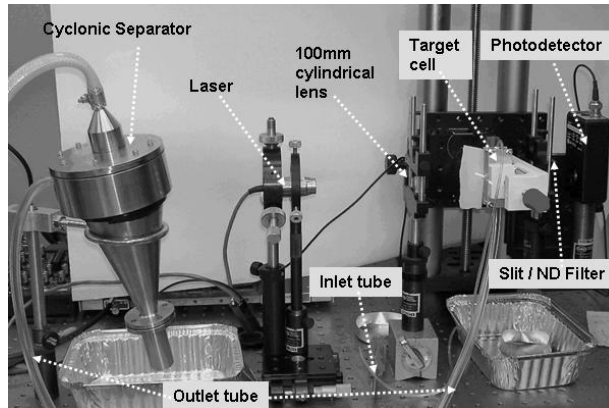


Figure 4. Experimental configuration of the TP-CAST

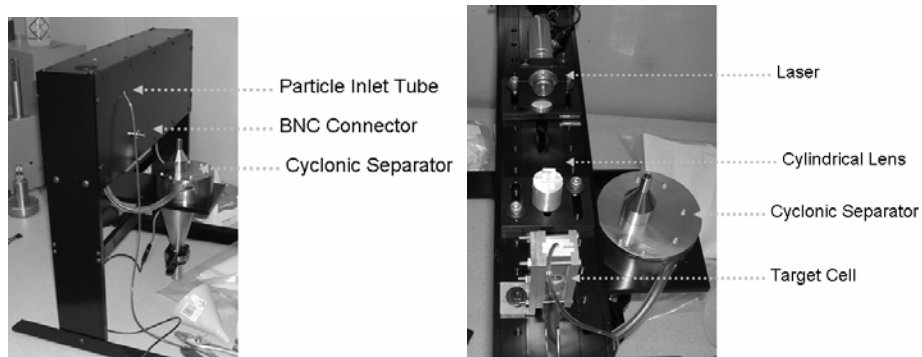


Figure 5. Completed TP-CAST instrument in light-shielding enclosure.

SOFTWARE DESIGN

The TP-CAST software is called “TP-CASTGUI” and is shown in Figure 6. TP-CASTGUI controls acquisition and processes particle “events”, where an event is a sudden change in the level of light collected on the photo receiver. We define this baseline level of light, where no sphere is blocking the laser light, as BL (the B x L term in Equation 4). There are five main steps to data acquisition. The first step is designation of various parameters (ADC gain, trigger fraction to start an event, etc.). Many of these parameters allow a level of noise immunity by controlling how an

event is identified. When a buffer has been acquired, the software searches the acquired data for a point where the signal level is below $BL \times \text{“trigger fraction”}$ and above $BL/2$. Every data point after this point is recorded until the signal is greater than $BL \times (\text{“trigger fraction”} + 0.01)$. The data between these points is determined to be an event only if the smallest level is below the minimum dip level defined as $BL \times \text{“min fraction”}$.

The second step is the optional determination of the beam profile. In this step, the user moves the photo receiver and a mounted slit along the beam line. The beam intensity is measured and a resulting profile is shown in a dialog box. The operator can find a position where the beam is uniform across the target cell aperture as measured by the mean and standard deviation.

The third step is computing the baseline value. This is done by simply switching to baseline mode and hitting the start button. A single buffer of 50,000 points (0.01 second) is acquired and averaged to yield a “constant baseline” value.

The fourth step is calibration. Multiple spheres of known size are passed through the system. When the user-entered number of calibration spheres is complete, the system computes an ideal scaling factor by finding the average difference between the constant baseline value and the minimum value of each calibration event.

Finally, the fifth step is measurement. The acquisition is started and spheres are collected. The software reports various counts including the number of events found. Each event may be plotted in real-time. The TP-CASTGUI screen during measurement is shown in Figure 6.

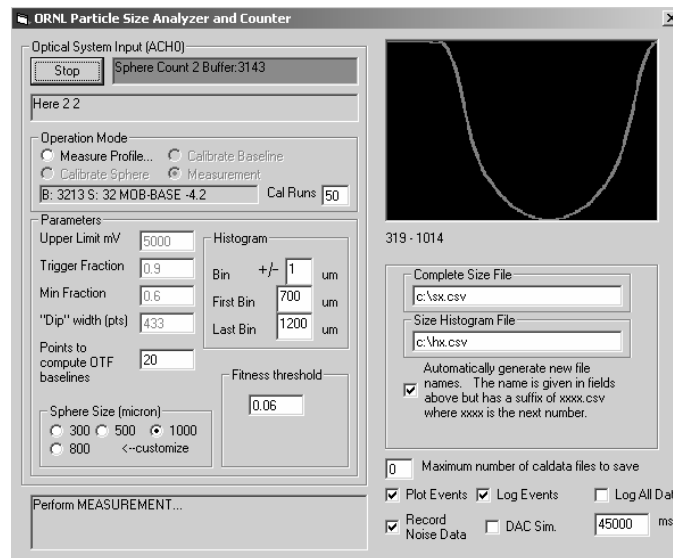


Figure 6. TP-CASTGUI during measurement. A continuous count of buffers, seconds, and particles is shown.

When the acquisition is finished by the user, the software writes a series of data files and shows the final estimated mean and standard deviation of the spheres. Output files include a histogram of the

event sizes, a measurement data file showing data on each event, and a “raw event” file that has the raw data for each event.

ACCOUNTING FOR NON-IDEAL ISSUES

Limited ADC Quantization

The error in our measurement can be limited by ADC resolution since we are trying to estimate the radius with the intensity of the obstruction. We attempt to better estimate the peak location by fitting the data to a parabola. In our software this is accomplished by finding the sampled peak, then locating 80 values on either side of the peak. These 161 values are used to find the coefficients of a least-squares error fit to a parabola and estimate the “true” minimum value of the curve. Since the number of values used is fixed, we need not compute the least-squares pseudo-inverse in real-time. We anticipate that different sized spheres would use different pseudo-inverse values, since the parabolic estimate is not as good away from the peak and smaller spheres may not provide 161 values for the estimate.

Parabolic Test for Detecting Counting Errors

The target cell was designed for 1000 micron spheres. When smaller spheres (800 micron) pass through the cell, some overlapping can occur. An example is shown below in Figure 7.

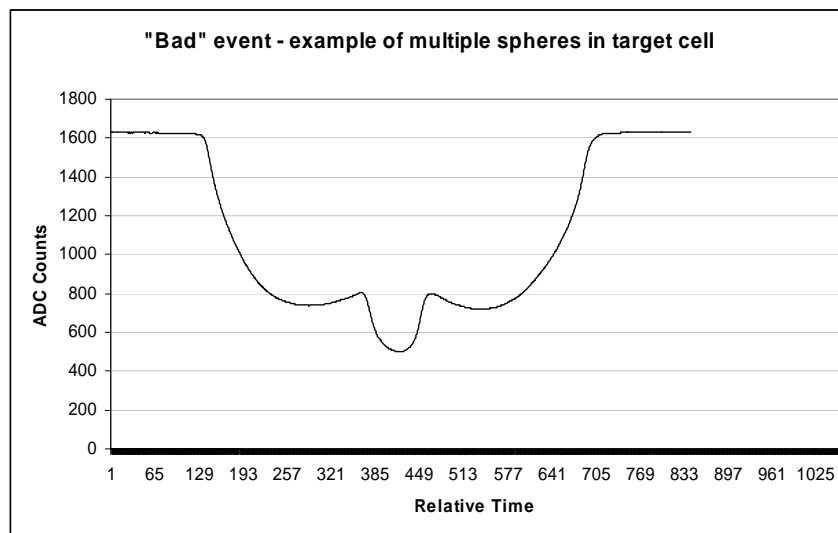


Figure 7. Example of an event with multiple particles.

In real-time, we determine the error between a 3-point parabolic fit and the event. Large errors indicate possible multiple events. This provides an easy-to-compute method for finding multi-particle events that can be manually screened with the help of additional software. The three-point fit consists of taking equally-spaced points from the event. These are fit to a parabola, and then every 100th point in the event is compared to its parabolic estimate. The total error is computed and averaged after normalizing by the unobstructed value. In order to minimize this type of error, target cells need to be designed for the particle size being tested.

Error in “Peak” Approximation

We performed simulations to study the error associated with just using the maximum signal peak and assuming it to be proportional to the radius. We used the equation (2) for the curve for $h = 50, 100, \text{ and } 150$ microns, with sphere sizes of 300, 500 and 1000 micron diameter. Then we varied the radius by ± 50 microns around the calibration diameters, measured the equation peak, and used the calibration peak and actual diameter to scale the values. The error in microns is shown in Figure 8 for the 300 micron sphere (the worst case scenario). In all cases, the value is less than 2 micron for $h < 50$ microns. Therefore, the laser slit size of 35 microns should not be a significant source of error in our measurements.

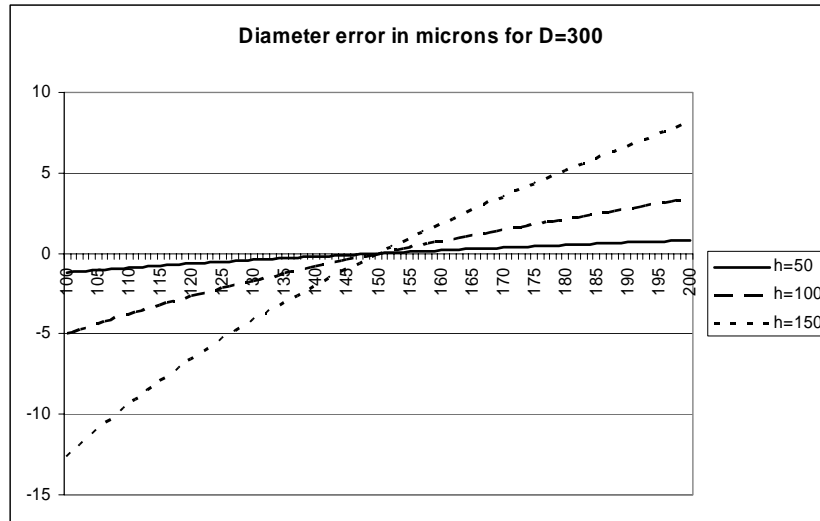


Figure 8. Error in small- h approximation for 300 micron sphere.

Fan Angle of Laser Line Generator

With an expanding beam, there are “bad zones” near the edges of the target cell where light blocked by a sphere is not collected by the photo receiver (Figure 9). Spheres that pass through these zones will attenuate less light than an identical size sphere through the center of the cell. We elected to minimize the impact of this effect by collimating the beam with a cylindrical lens.

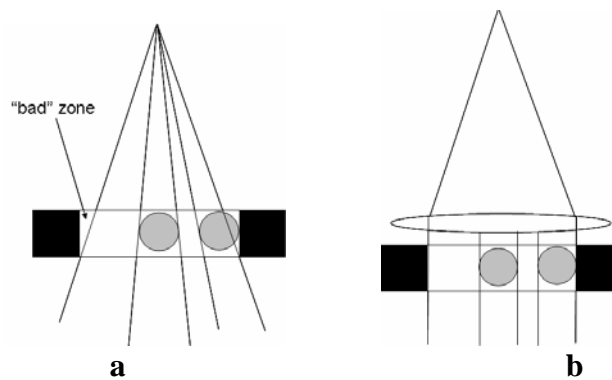


Figure 9. Illustration of (a) fan angle problem. (b) solution with cylindrical lens.

Bias and Laser Drift

Although the baseline value B in Equation 4 is not a function of time, we would like to determine how to account for changes in B over time. As this level increases or decreases, the light that is passed around a sphere that obstructs the laser would seem to increase or decrease, so long as the minimum level still passes some light. Another problem that can arise is a bias term which is not attenuated by a passing sphere. We can remove $B(t)$ by normalizing the signal by a computed instantaneous $B(t_0)$, so long as $B(t)$ is not a rapidly changing function of time. We can remove the bias effect by computing the value of $B(t)$ prior to each measurement and subtracting it from the overall result. We report on experiments to determine which model is the most likely source of error in the Experimental Results section of this paper.

We implemented two techniques to compute instantaneous $B(t_0)$:

On-The-Fly or OTF – in this case, several points are taken prior to an identified event and averaged to compute $B(t_0)$.

Mean-of-Buffers or MOB – if a buffer (50k points) does not contain an event, we average every 10th value (for 5,000 total data points). When a buffer does contain an event we use the previously computed MOB value for $B(t_0)$.

All total, we therefore implemented 10 different ways of computing the size using the peak value.

Constant Base Line or CBL – use the value computed during the “baseline” phase for all measurements

OTF – use the On-the-Fly method to compute B and subtract the minimum value from this B .

MOB – use the Mean-Of-Buffers method to compute B and subtract the minimum value from this B .

OTFN (On-The-Fly Normalized) – use the On-the-Fly method to compute B and divide the signal by this B .

MOBN (Mean-Of-Buffers Normalized) – use the Mean-Of-Buffers method to compute B and divide the signal by this B .

The final five methods are identical to the techniques above except we replace the minimum with the estimated minimum by using a parabolic least-squares-fit to the curve; we identify them as CBLEST, OTFEST, MOBEST, OTFNEST, and MOBNEST.

Beam uniformity

To assess beam uniformity, we inserted a slit before the photo receiver and moved the target cell, slit, and photo detector across the beam to measure the profile. At each measurement point the signal was integrated for 0.01 seconds (50,000 points) to avoid time-dependent drifts. We then determined the best region of the curve by taking each point, assuming it was the position of calibration, computed a scaling constant for that position, then applied the scaling constant for the beam profile measurements at +/- 0.75 mm on either side (because the target cell aperture is 1.5 mm). While the uniformity profile was not identical each time, it showed a very similar shape from run to run. A typical profile and accompanying mean and standard deviation estimate are shown in Figure 10. For this example, we see that the best estimated position is 16.00 mm, where the mean error is 2.28 microns and the standard deviation is 5.27 microns.

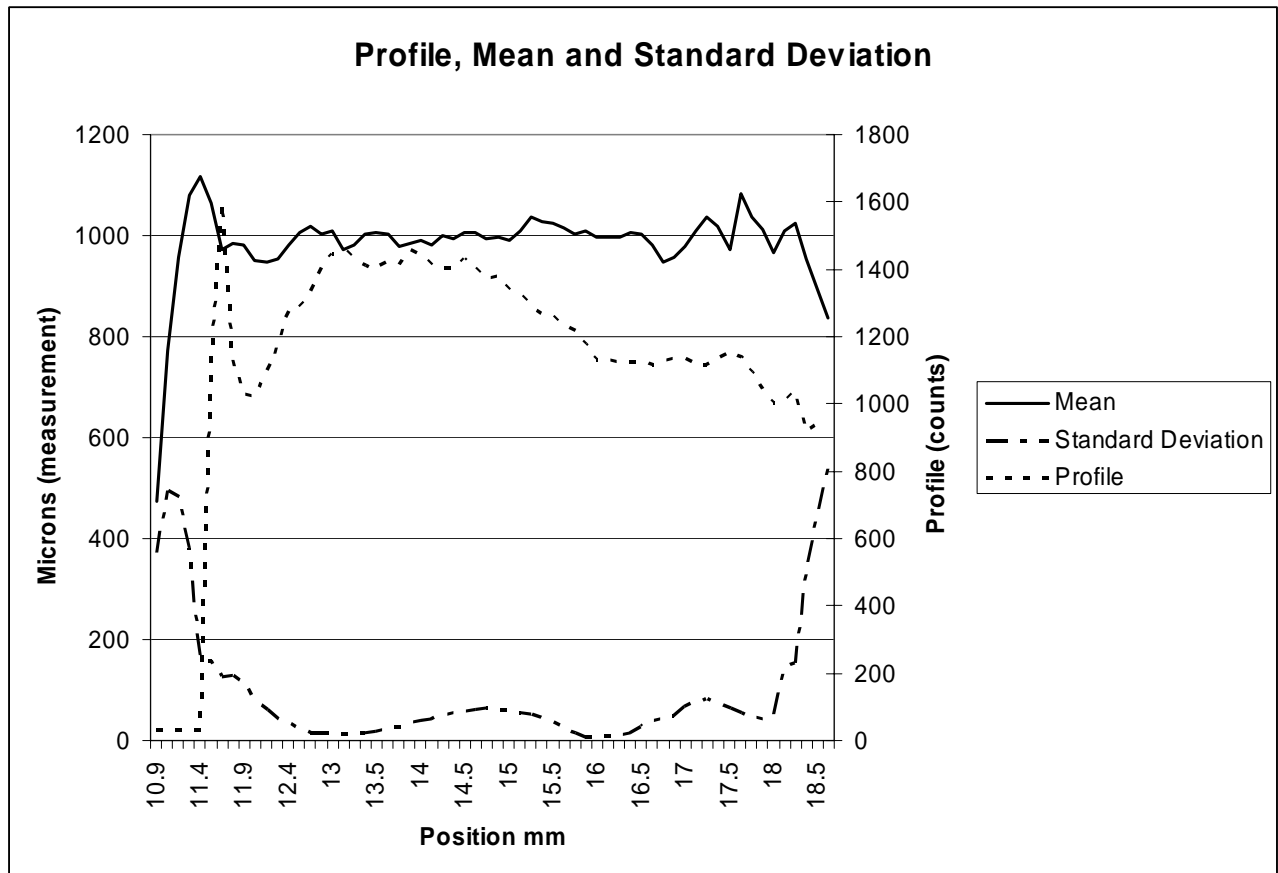


Figure 10. Beam profile, estimated mean and standard deviation as a function of the target cell position for the experimental system.

EXPERIMENTAL RESULTS

Experiments were run using 1000 micron diameter stainless steel spheres. Two sets of spheres with counts of 500 and 95 were utilized. The smaller set was used for calibration by setting the TP-CASTGUI software to use 50 calibration runs. Counts of 500 spheres were obtained consistently for 10 consecutive trials. The 95 spheres were measured with optical microscopy and image processing. The mean diameter of the set was found to be 1003.4 microns, with a maximum value of 1008 and a minimum of 999. The standard deviation of the set was 1 micron.

Counting Accuracy

To estimate the probability of error, we used an exact method based on the binomial distribution for small error numbers [6] for a one-sided interval. In this procedure, to find the limit on the error for a $100 \times (1-\alpha)$ confidence level, we must solve the equation below, where N is the number of trials and N_d is the number of “defects” or errors.

$$\sum_{k=0}^{N_d} \binom{N}{k} p_u^k (1 - p_u)^{N-k} = \alpha / 2. \quad \text{Equation 5}$$

For our case, $N = 5000$ and $N_d = 0$. For a 95% confidence interval we let $\alpha = 0.05$. Therefore, we find $p_u = 7.4 / 10,000$. Thus, we can say, with 95% confidence, that the system will have a counting error less than 0.074%.

Size Estimation Algorithm Comparison

Our next step is to evaluate and compare the three algorithms for estimating the size. We performed a comparison of the peak, square and integral algorithms described earlier by taking runs of 500 particles, using the first 50 to establish a calibration constant (assuming a particle size of 1000 microns), and then applying the algorithms off-line. Although simulated results showed improvement in the standard deviation (SD) when using the square and integral techniques, our experimental results did not show much improvement between the different estimation algorithms.

Table 1. Comparison of different size estimation algorithms.

Count	Peak D	Peak SD	Square D	Square SD	Integral D	Integral SD
450	999.1	11	998.8	10	999.3	10
450	999.9	12	1000.1	12	1000.5	10
450	1000.2	9	1000.1	9	1000.5	8
450	1000.5	11	1000.6	11	1000.8	10
450	999.6	11	999.7	11	1000.1	10
450	999.6	10	1000.2	10	1000.4	9
450	1001.9	10	1001.9	10	1002.3	9
450	1000.0	8	1000.1	8	1000.5	7
450	1001.2	9	1001.6	9	1001.8	8
450	997.2	9	996.9	9	998.1	8

Baseline Drift Modeling Comparison

Figure 11 compares different baseline models. We found the mean size estimate for each signal model and reported the mean error and standard deviation. We plotted the average error across all runs and average standard deviation across all runs. The MOBESTN method seems to be the best overall technique, but we plan to conduct more experiments, especially over longer time periods. Based on the standard deviation, the error is approximately +/- 11 microns for the MOBESTN method.

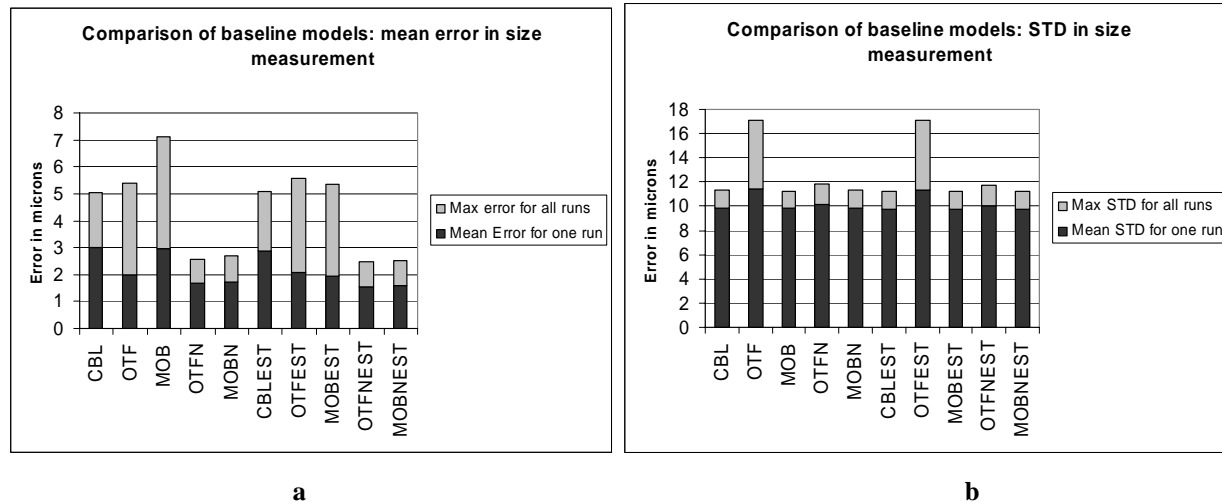


Figure 11. Comparison of different baseline models. a) max and mean of mean error over 10 runs of 500 spheres (1000 micron diameter) ; b) max and mean standard deviation.

CONCLUSION

The TRISO Particle Counting And Sizing Tool (TP-CAST) was developed for high-speed counting and size measurement of TRISO spheres of diameter from 300 to 1000 microns. We estimated the counting accuracy as less than 0.075% error with a 95% confidence. The TP-CAST size measurement accuracy was on the order of 11 microns standard deviation for spheres 1000 microns in diameter. The main sources of error in the size distribution measurement are believed to be beam uniformity and electronic / optical noise. Despite simulations indicating alternate algorithms could improve performance, we found that the best method for estimating size was to simply take the minimum value of an obstruction signal. Modifications to the “peak estimation” algorithm that accounted for varying baseline levels caused by either bias changes or changing laser intensity were not consistently better than the simple “constant base line” model for our experiments, but additional experiments must be done to determine if this result holds for longer time periods. Finally, although the current particle transport system does not support the maximum detection rate, electronically generated data showed rates of 200 particles per second, implying a throughput of 720,000 particles per hour.

REFERENCES

- ¹ ORNL Review Vol. 35, No. 2, 2002
- ² R.N. Morns, D.A. Petti, D.A. Powers, and B.E. Boyack, “TRISO-Coated Particle Fuel Phenomenon Identification and Ranking Tables (PIRTs) for Fission Product Transport Due to Manufacturing, Operations, and Accidents (NUREG/CR-6844)”, July 2004, available at <http://www.nrc.gov/reading-rm/doc-collections/nuregs/contract/cr6844/>
- ³ K. Wallisch and P. Koss, “Automatic size analysis of coated fuel particles,” Nucl. Tech. 35 (1977) 279-283
- ⁴ J. Price, J. Hunn. “Optical Inspection of Coated Particle Nuclear Fuel,” in Proceedings of Machine Vision Applications in Industrial Inspection XII, SPIE vol. 5303, pp. 137-149, January 2004.
- ⁵ R. Hockey, L.J. Bond, C. Batishko, J.N. Gray, J. Saurwein, and R. Lowden, “Advances in Automated QA/QC for TRISO Fuel Particle Production,” Proceedings of ICAPP '04, Pittsburgh, PA USA, June 13-17, 2004; Paper 4213
- ⁶ NIST Engineering Statistics Handbook, <http://www.itl.nist.gov/div898/handbook/prc/section2/prc241.htm>